processes

MDPI

Article

The Influence of the Application Layer of Pouring Semi-Flexible Pavement Material on Low-Temperature Stress

Guoxun Li [1], Deyong Wang [1], Huaizhi Zhang [2,*], Biao Xu [1], Fan Yang [3] and Zhen Zhang [2]

[1] China First Highway Engineering Co., Ltd., Beijing 100124, China; 18580513226@163.com (G.L.); wang1de2yong@126.com (D.W.); xtender0209@163.com (B.X.)
[2] School of Transportation and Geomatics Engineering, Shenyang Jianzhu University, Shenyang 110168, China; zz1192374834@163.com
[3] CCCC Comprehensive Planning and Design Institute Co., Ltd., Beijing 100124, China; sjzxfy@126.com
* Correspondence: huaizhizhang@163.com

Abstract: Pouring semi-flexible pavement material (PSFM) is widely used as a wearing layer material or below pavement due to its excellent resistance to deformation at high temperatures and under heavy loads. However, in cold regions, the material exhibits severe cracking issues. The primary objective of this study is to enhance the resistance of pouring semi-flexible pavements (SFPs) to low-temperature cracking in cold regions by strategically designing pavement structures that incorporate PSFM. To achieve this goal, we conducted indoor tests to determine the relaxation modulus and temperature shrinkage coefficient of PSFM and simulated a pavement structure using COMSOL finite element simulation. The impacts of different application layers and layer thicknesses on low-temperature stresses were investigated based on these findings. The research findings indicate that when PSFM is used as the wearing layer material, the low-temperature stress is 4.7% lower than that of typical materials used in the pavement-wearing layer. When used as the binder layer material, the low-temperature stress on the wearing layer material increases by 3.5%. As the thickness of the wearing layer increases, the low-temperature stress within the pavement structure decreases, but the low-temperature stress on the pavement surface increases. Therefore, it is recommended to use PSFM as the binder layer material and appropriately increase the thickness of the wearing layer to enhance the pavement's resistance to low-temperature cracking.

Keywords: application layer; pouring semi-flexible pavement material; low-temperature stress

Citation: Li, G.; Wang, D.; Zhang, H.; Xu, B.; Yang, F.; Zhang, Z. The Influence of the Application Layer of Pouring Semi-Flexible Pavement Material on Low-Temperature Stress. *Processes* **2024**, *12*, 245. https://doi.org/10.3390/pr12020245

Academic Editor: Dicho Stratiev

Received: 31 December 2023
Revised: 16 January 2024
Accepted: 22 January 2024
Published: 24 January 2024

1. Introduction

Pouring Semi-Flexible Pavement Material (PSFM) constitutes a composite material achieved by pouring cement-based grouting material into a porous asphalt mixture characterized by porosity levels typically falling within the range of 18% to 28% [1]. Renowned for its exceptional load-bearing capacity, durability, and extensive fatigue life [2–4], PSFM finds widespread application in pavement construction. Its efficacy in addressing challenges posed by high-temperature, heavy loads has been well documented [5,6]. The research and application of PSFM have experienced steady growth since its introduction in China during the 1980s [7,8]. As of 2022, 14 provinces and municipalities, including Jiangsu, Shanghai, Guangdong, and Hubei, have embraced PSFM as the wearing layer material in various urban infrastructures such as arterial highways, intersections, and bus stops. This adoption has notably mitigated issues related to rutting, waviness, and surge. In settings like service areas and toll stations, traditional cement concrete pavement has encountered challenges like peeling, exposed aggregate, and cracks, primarily due to frequent vehicle acceleration and deceleration. The integration of PSFM as an overlay in such locations has yielded remarkable results in engineering applications. In other projects employing PSFM for different layers, the pavement has demonstrated noteworthy resistance to rutting.

This underscores the transformative impact of PSFM on enhancing the performance and longevity of pavement structures in diverse scenarios.

PSFM enhances heat tolerance and structural strength with the integration of pouring cement-based grouting material in which PSFM is applied as a pavement material in the pavement structure to give the pavement a rigid–flexible character; this pavement is called pouring semi-flexible pavement (SFP) [9,10]. However, its susceptibility to low temperatures renders the cement-based grouting material prone to brittleness, leading to shrinkage deformations and eventual cracking within the weak interface shared by asphalt and the cement-based grouting material [11,12]. Consequently, the low-temperature resilience of PSFM proves inferior to that of other asphalt mixtures [13,14]. In winter, cold regions experience low temperatures and substantial daily temperature fluctuations, contributing to material shrinkage and deformation within pavements. To assess the practical viability of SFPs in the cold region, a field investigation scrutinized SFPs in Liaoning province after years of operation. The SFPs predominantly featured a stone–mastic asphalt mixture (SMA-13) as the wearing layer material and PSFM as the binder layer material. A contemporaneous high-modulus asphalt pavement (HMAP), constructed using SMA-13 and a high-modulus asphalt mixture (HMM-20), served as a comparative reference. Figure 1 visually delineates the identical diseases present in both pavements. Compared with the HMAP, detailed further in Table 1, the investigation revealed that the longitudinal crack rate of the two SFPs measured 54 m/km and 218 m/km, marking a 38% reduction. Additionally, the transverse crack rate increased by 14 lines/km and 34 lines/km over the HMAP. Rutting experienced a decrease of 3 mm. While the area exhibiting block cracks in the SFPs was smaller than that of the HMAP, it is notable that one of the SFPs manifested alligator cracking. This investigation underscores PSFM's potential to enhance a pavement's rutting resistance, albeit at the expense of heightened susceptibility to temperature fluctuations.

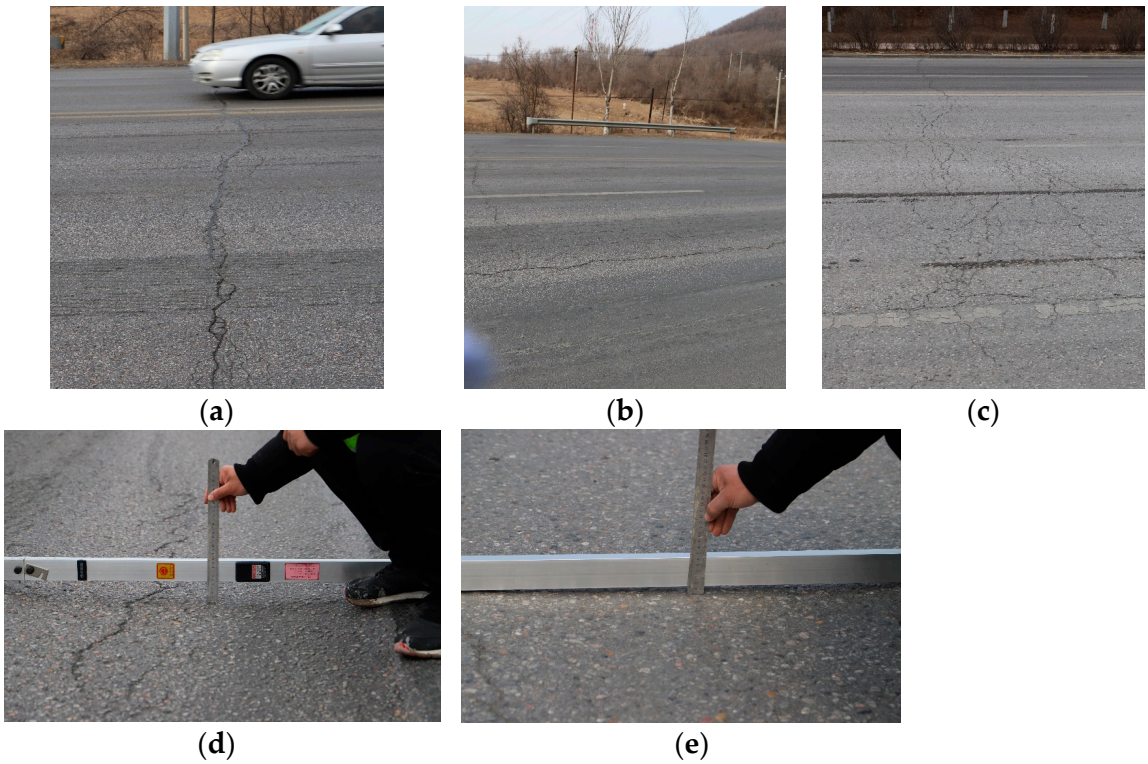

Figure 1. (**a**) For transverse cracking; (**b**) for longitudinal cracking; (**c**) for alligator cracking; (**d**) for HMAP pavement rutting; and (**e**) for SFP pavement rutting.

Table 1. Pavement field survey and main disease types.

Pavement Type	Pavement Structure	Pavement Performance Characteristics				
		Transverse Crack Rate (line/km)	Longitudinal Crack Rate (m/km)	Rutting (mm)	Block Crack (m^2)	Alligator Crack (m^2)
SFP	4 cm SMA-13 + 6 cm PSFM	52	54	9	6	
HMAP	4 cm SMA-13 + 6 cm HMM-20	18	92	12	13	
SFP	4 cm SMA-13 + 5 cm PSFM	110	218	9	10	6
HMAP	4 cm SMA-13 + 5 cm HMM-20	96	337	12	11	

In understanding the critical factors influencing the cracking propensity of SFP, it becomes imperative to delve into the underlying mechanisms governing their cracking behavior. Utilizing image processing techniques, the spatial arrangement of the constituent phases—comprising materials and voids—within PSFM has been discerned and segmented into grids to facilitate numerical simulations. Wang [15] noted that the volumetric changes, particularly the expansion or contraction of the cement-based grouting material, engender tensile stresses within the composite material. Notably, lower temperature-induced contractions pose a significantly higher risk to the structural integrity of PSFM. Moreover, Jiang [16] established the influence of dynamic loading on the mechanical properties of PSFM, leading to stress concentrations and fatigue-induced damage, particularly at weak areas of contact between the asphalt and aggregate. Concurrently, Xiong [17] developed an ANOVA model, corroborating the significant impact of surface temperature on the cracking behavior of PSFM. When the shrinkage stress surpasses the material's tensile strength, it invariably leads to impaired interlayer bonding and subsequent cracking [18]. Hence, to enhance the cracking resistance of SFP, especially in cold regions, and thereby extend the material's service life, a thorough analysis of low-temperature stress within the pavement structure is imperative before incorporating PSFM.

In anticipation of undertaking a low-temperature stress analysis of SFP, a comprehensive examination of the material properties of PSFM is imperative. Porous asphalt mixtures exhibit stress relaxation, and the relaxation modulus serves as a prevalent indicator of the relaxation properties inherent in linear viscoelastic materials [19–22]. Although various test methods are available for validating the relaxation modulus, the intricacy and challenges associated with the relaxation test process render it an incomplete measure of the viscoelastic characteristics of asphalt mixtures [23–25]. To address this limitation, this study ascertains the relaxation modulus of PSFM through dynamic modulus testing, employing the principle of time–temperature superposition [26–28]. This method involves the transformation of frequency domain–dynamic modulus relationship curves into time domain–relaxation modulus principal curves expressed using the Prony series. These curves serve to delineate the constitutive relationship of respective mixtures within the linear viscoelastic range [29,30]. This holistic methodology significantly advances our comprehension of the viscoelastic characteristics inherent in PSFM and substantively contributes to a more sophisticated approach to pavement structural design, particularly within the framework of addressing low-temperature stress considerations for SFP.

It becomes crucial to integrate the temperature shrinkage coefficient of the cement-based grouting material into the overall temperature stress analysis [31]. Hao [32] conducted a thorough investigation into the temperature shrinkage coefficient of PSFM through numerical modeling. The findings reveal that the incorporation of cement-based grouting material does not impart any significant alteration to the overarching temperature shrinkage coefficient of PSFM. However, the low-temperature cracking of PSFM is mainly caused by cement-based grouting material. Therefore, it is noteworthy that the temperature shrinkage coefficient of PSFM exerts a direct influence on the temperature shrinkage strain experienced by the wearing layer, consequently impacting the resultant low-temperature stress.

The analysis of SFP low-temperature stress is based on the analysis method of asphalt pavement. Hills and Brien [33] approached their study on the assumption of isotropic pavement materials, positing a uniform distribution of temperature stress with a seamless connection between layers. Zheng [26] adopted an iterative finite element approach, establishing an equation for the temperature stress field under continuous cooling conditions. This approach facilitates the calculation of stress distribution with variations in temperature. In a related vein, Geng [34] proposed a method for analyzing temperature stresses in asphalt pavements under dynamic loading. This method, rooted in the viscoelastic theory of asphalt mixtures, accounted for the nonlinear variation in temperature with time and depth of the asphalt layer, thereby deriving temperature stresses at different locations and temperatures. Collectively, these studies contribute to a comprehensive understanding of temperature stress analysis methodologies for asphalt pavements, with implications for both design and practical applications. Si [35] leveraged the viscoelastic properties inherent in asphalt mixtures to formulate a nonlinear governing equation for coupled heat–liquid force. This formulation involved a comparative analysis with a single stress field, revealing that internal stresses within the pavement exhibit an augmentation when temperature and water infiltration considerations are incorporated. In a parallel exploration, Zhang [36] contributed to the field by developing a numerical computational model characterizing the temperature stress field over time. Notably, this model extends the understanding of material properties by integrating the relaxation properties of the asphalt surface material as a mechanical parameter for finite element analysis. Additionally, Fang [20] made noteworthy contributions by refining the calculation formula for cumulative temperature stress in asphalt pavement. The comprehensive elucidation incorporates considerations of asphalt stress characteristics, presenting a thorough process and calculation formula. Emphasizing the material's shrinkage strain underscores its greater influence on performance compared with vehicle loads.

In synopsis, extant investigations have exhibited a dearth of comprehensive analysis concerning temperature stresses in SFP. Traditional parameters, exemplified by the dynamic modulus, prove inadequate for ensuring precise damage detection and the evaluation of pavement structure performance. Consequently, there exists a compelling need for further inquiry to enhance the accuracy of pavement performance assessment.

In the present study, we address this gap by incorporating the measured relaxation modulus and temperature shrinkage coefficient of PSFM under low-temperature conditions. Utilizing these data, we develop a finite element simulation in COMSOL for the pavements that introduce PSFM. This simulation model facilitates the evaluation of low-temperature stress distribution in pavements with diverse structures exposed to varying temperature conditions. A comparative analysis is executed employing a representative asphalt pavement structure. The purpose of this study is to explore the subtle effects of PSFM application layer and thickness on pavement low-temperature stress caused by low temperature. The outcomes of this study offer valuable insights and guidance for the nuanced design of SFP structures, particularly in cold regions. By systematically addressing the limitations of existing approaches, this research contributes to advancing understanding and design considerations for SFP. The main content of this study is shown in Figure 2.

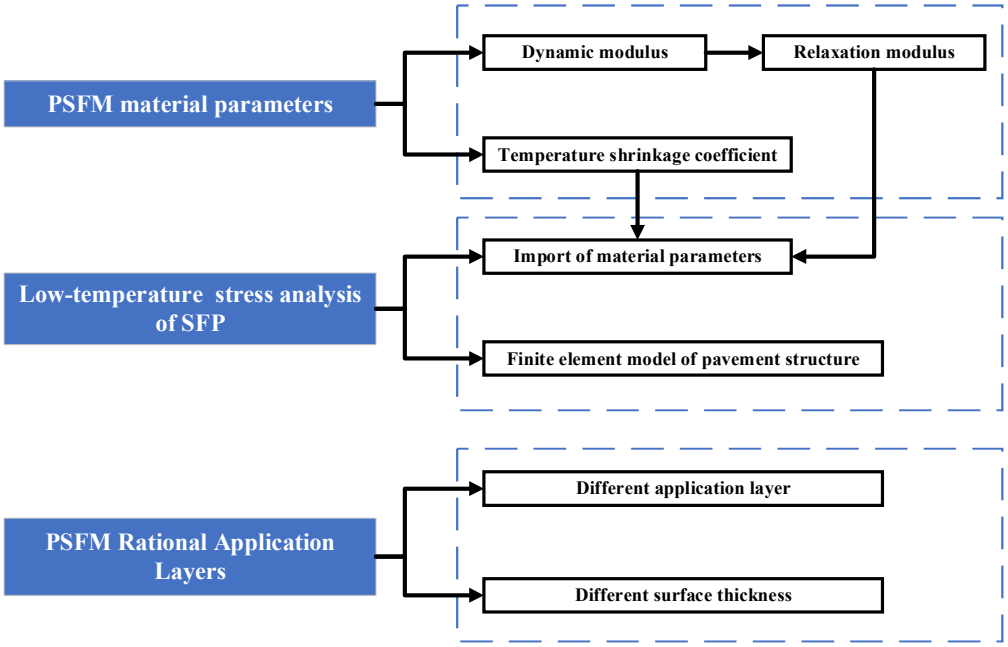

Figure 2. The main research contents of this study.

2. Materials and Test Methods

Due to the lack of standard values for the actual performance of PSFM materials at low temperatures, it is easy to deviate from the actual situation when performing finite element analysis of SFP low-temperature stress. Therefore, in this section, by preparing PSFM specimens that meet the requirements, laboratory tests are carried out to obtain dynamic modulus values at different temperatures and frequencies, and temperature shrinkage coefficients at different temperature ranges.

2.1. Raw Materials

In this study, the porous asphalt mixture, in reference to the international technical specification (AASHTO M323), is composed of SBS-modified asphalt and open-graded aggregates. In the technical specification of SBS-modified asphalt tests, we refer to international standards: asphalt penetration tests from ASTM D5, softening point tests from ASTM D36, and ductility tests from ASTM D113. The particle size distribution of the aggregates is presented in Table 2, and the basic properties of the SBS-modified asphalt are shown in Table 3. The oil–stone ratio of 4.4% is determined through the Marshall stability test, corresponding to an average void ratio of 22%.

Table 2. Aggregate particle size distribution of porous asphalt mixtures.

Particle Size (mm)	19	16	13.2	4.75	2.36	0.6	0.3	0.15	0.075
Percentage passing (%)	100	96.2	84.7	18.3	16.2	8.0	5.8	4.7	3.2

Table 3. Technical indices of SBS-modified asphalt.

Testing Indexes	Test Result	Design Requirements
Penetration at 25 °C, 100 g, 5 s (0.1 mm)	56.8	40–70
Softening point (°C)	32.2	≥25
Ductility at 5 °C (cm)	75.9	≥70

Through the test mixing of grout for PSFM, the final determination of the water–cement ratio, water:grout = 0.29:1, the performance indicators are shown in Table 4.

Table 4. Basic properties of cement-based grouting materials.

Testing Indexes		Test Result	Design Requirements
Mobility (s)		12.9	10~18
Dry shrinkage (%)		0.11	≤0.3
Flexural strength (MPa)	3 h	2.3	≥2
	7 d	4.7	≥4
	28 d	7.9	≥7
Compressive strength (MPa)	3 h	13.5	≥7
	7 d	28.9	≥20
	28 d	42.6	≥35

2.2. Specimen Preparation

According to the Chinese technical specifications (JTG E20-2011), utilizing the T0738-2011 test method, the initial steps involve the preparation of asphalt mixture specimens characterized by large voids. These specimens possess a molding diameter of 150 mm and a height of 170 mm, achieved through the utilization of a gyratory compactor. Following the cooling of the specimens to room temperature, they underwent demolding and subsequent sealing with plastic encompassing the specimen perimeter and bottom base. The next phase entails the uniform mixing of a specially designed cement-based grouting material, which is subsequently poured into the porous asphalt mixture specimens. To facilitate the penetration of cement-based grouting material, a vibrating table and vacuum compressor are employed during production, ensuring thorough filling of voids within the porous asphalt mixture. The treated specimens are then subjected to standard maintenance conditions for a duration of three days to achieve the requisite curing. Following this curing period, cores are extracted from the specimens, and samples are precisely cut to meet specified dimensions: a diameter of 100 ± 2 mm and a height of 150 ± 2.5 mm. According to the specification, the number of a group of asphalt mixture specimens is not less than four. In order to ensure the accuracy of the test results, in this section, we prepare five specimens, test them respectively, and take the average value as the result. The specific steps are shown in Figure 3.

Figure 3. PSFM specimen preparation.

2.3. Test Methods

2.3.1. Dynamic Modulus Test

This investigation adheres to the guidelines set forth in Chinese technical specifications (JTG E20-2011) with the primary objective of conducting a dynamic modulus test on a PSFM, employing the DTS-30 testing machine. To facilitate this test, metal terminals were affixed to the external surface of the sample using AB adhesive, ensuring the secure attachment of the displacement transducer. The driving speed is one of the main reasons affecting the frequency of load action. The selection of test load frequency should be included in the

applicable scope of the road as far as possible. Therefore, the range of test load frequency of 0.1 Hz, 0.5 Hz, 1 Hz, 5 Hz, 10 Hz, and 25 Hz can include the actual driving speed of vehicles on the road.

The experimental procedure encompassed the systematic measurement of dynamic modulus values for semi-flexible asphalt mixtures across a range of temperatures (−10 °C, 5 °C, 20 °C, 35 °C, and 55 °C) and at various frequencies (0.1 Hz, 0.5 Hz, 1 Hz, 5 Hz, 10 Hz, and 25 Hz). The experimental step is visually presented in Figure 4. This methodical approach aligns with the standards outlined in JTG E20-2011, ensuring the rigor and academic integrity of the dynamic modulus testing conducted on semi-flexible asphalt mixtures.

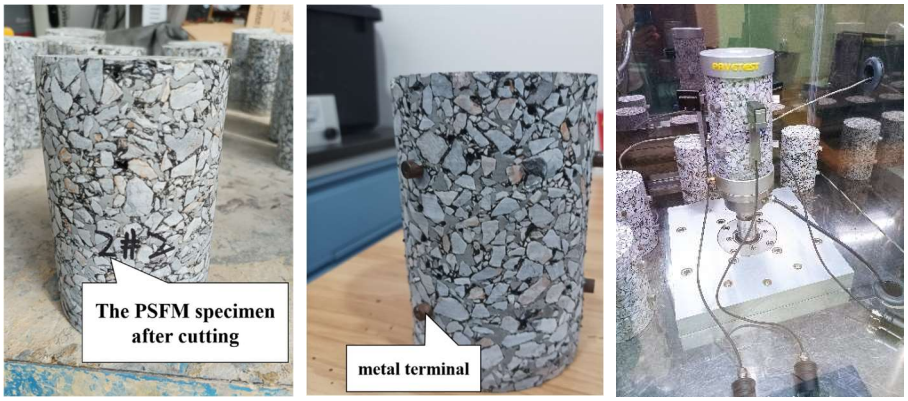

Figure 4. Dynamic modulus test of PSFM.

The dynamic modulus (E^*) and phase angle (φ) were obtained from tests under various conditions. The E^* represents the stress and strain ratio required to reach a steady state, while the phase angle is determined by the time at which the strain lags the stress. The storage modulus (E') and loss modulus (E'') were determined through Equation (1).

$$\begin{cases} E' = |E^*| \cos \varphi \\ E'' = |E^*| \sin \varphi \end{cases} \quad (1)$$

The logarithmic Sigmoidal function model [37] was utilized in this study to determine the dynamic modulus master curves. The equation representing the Sigmoidal function is shown in Equation (2):

$$\lg E' = a + \frac{b}{(1 + \lambda e^{c+d\lg f})^{\frac{1}{\lambda}}} \quad (2)$$

where a represents the logarithm of the smallest stored modulus value; b represents the logarithm of the stored modulus range (maximum modulus value minus minimum); c and d are the parameters of the Sigmoidal function; and λ denotes the shape of fitted curves. $\lambda = 1$ signifies the logarithmic Sigmoidal function with a symmetric relationship, whereas $\lambda \neq 1$ represents the generalized logarithmic Sigmoidal function. Additionally, f represents the loading frequency at the reference temperature. The shift factor is calculated using the WLF in Equation (4):

$$\lg f = \lg f_0 + \lg a_T \quad (3)$$

$$\lg a_T = \frac{-C_1(T - T_r)}{C_2 + (T - T_r)} \quad (4)$$

where f_0 is the loading frequency at temperatures other than the current; a_T is the shift factor, which depends on temperature; T is the temperature being tested; T_r is the reference temperature; and C_1, C_2 are terms that remain constant.

2.3.2. Temperature Shrinkage Test

Conforming to Chinese technical specifications (JTG E51-2009), the formation of cement-based grouting material specimens is achieved through the rutting test specimen molding method. After this, a cutting machine is employed to precision-shape the specimens to meet specified dimensions: length × width × height = 40 mm × 40 mm × 160 mm. The application of electrical resistance strain gauges to the specimen surface, facilitated by 502 adhesives, is a critical step in the experimental procedure. Following the curing process, a layer of waterproofing agent is meticulously applied and allowed to solidify before the connection of wires. See Figure 5 for specific steps.

(**a**) (**b**)

Figure 5. (**a**) LMT-2 test incubator used for temperature shrinkage test; (**b**) specimen after applying strain gauges.

For temperature compensation, microcrystalline glass is utilized. The experimental setup utilizes the LMT-2 test incubator equipped with temperature control settings, encompassing a temperature range from −25 °C to 15 °C. The temperature variation is structured in intervals of 5 °C, initiating from lower temperatures and progressing in 10 °C increments within the range of −25 °C to −15 °C. Each interval involves a gradual increase and subsequent maintenance of constant temperature for 1–2 h. During these intervals, the temperature shrinkage strain of the specimen is recorded systematically. Subsequently, the temperature shrinkage coefficient of the cement mortar is derived for different temperature intervals. The final step involves the computation of the temperature shrinkage coefficient for each temperature interval based on the acquired test results. The ensuing test data undergo processing according to a specified formula, as outlined in Equation (5), to derive meaningful insights from the experimental outcomes:

$$\beta = \frac{\Delta\varepsilon}{\Delta t} + \beta_s \tag{5}$$

where β represents the strain caused by changes in temperature; $\Delta\varepsilon$ is the amount of strain measured in macrostrains that occurs as a result of a change in Δt, the temperature; and β is the coefficient for line shrinkage of the temperature-compensated sheet.

3. Obtaining the Properties of PSFM

3.1. Dynamic Modulus

Initially, the data underwent analysis utilizing Microsoft Office Excel 2022. The storage modulus values, essential to this study, are acquired under specified reference temperature conditions, set at 20 °C. Subsequently, these values undergo fitting to ascertain the coefficients a, b, c, and d. The determination of the shift factor (a_T) for the dynamic modulus curves at each temperature is achieved by substituting the values back into Equation (2).

As illustrated in Figure 6, a discernible linear relationship is observed among the a_T at different temperatures. This observation underscores the inherent viscoelastic properties of the PSFM, despite its composition containing a specific proportion of cement-based grouting material. The application of the a_T enables the horizontal adjustment of frequency

domain–dynamic modulus relationship curves under varying temperature conditions. The resultant dynamic modulus master curve is depicted in Figure 7, with corresponding coefficients presented in Table 5. This systematic approach ensures a logical progression in the analysis, emphasizing the viscoelastic behavior of the PSFM and providing a comprehensive understanding of the material's response under different temperature conditions.

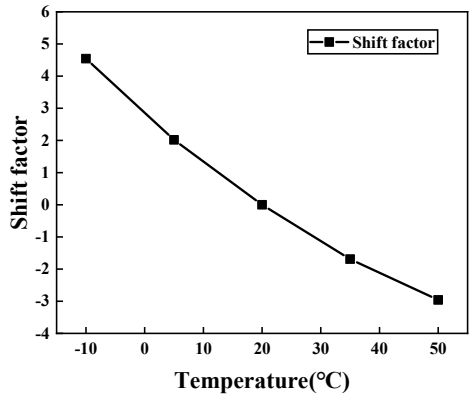

Figure 6. Shift factor (base 20 °C).

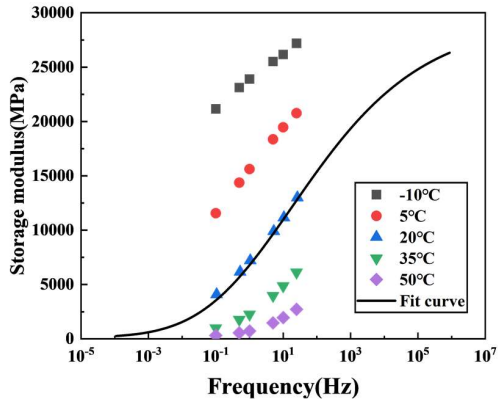

Figure 7. Dynamic modulus master curve.

Table 5. Coefficient values of the master curve.

Ratio	*a*	*b*	*c*	*d*	λ	C_1	C_2	Errors (%)
	1.193	3.281	−1.450	−0.455	0.639	21.410	177.202	0.67

3.2. Relaxation Modulus

The determination of the relaxation modulus in the frequency domain for asphalt mixtures during service, specifically in relation to stress relaxation, is achieved by applying the Boltzmann equivalent principle [38,39]. This process involves utilizing a discrete relaxation time spectrum method for the transformation of the time–frequency domain. Widely accepted within the field, the generalized Maxwell model is employed to characterize the relaxation behavior of asphalt mixtures, particularly within the linear viscoelastic range [40]. The representation of the relaxation modulus within the generalized Maxwell model is articulated through a Prony series, succinctly expressed in Equation (6). This systematic approach ensures a rigorous and comprehensive understanding of the asphalt mixture's behavior under stress relaxation conditions, providing a foundation for further analysis within the linear viscoelastic range:

$$E(t) = E_e + \sum_{n=1}^{N} E_n e^{-\frac{t}{\rho n}} \quad (6)$$

where $E(t)$ is the relaxation modulus based on the time domain, $E_e = E'|_{\omega \to 0^+}$ denotes the storage modulus when the angular frequency ω tends to 0, $\omega = 2\pi f$, E_n is the relaxation strength, and ρ_n is the discrete relaxation time.

The calculation of Equation (6) from the storage modulus produces a Prony series that is primarily influenced by the dynamic modulus master curve. This is then directly converted into the relaxation strength by the storage modulus, resulting in Equation (7).

$$E'(\omega) = E_e + \sum_{n=1}^{N} \frac{\omega^2 \rho_n^2 E_n}{\omega^2 \rho_n^2 + 1} \tag{7}$$

In this study, a discrete relaxation time spectrum method is employed, wherein configuration points are predefined to achieve alignment between measured and computed values. The determination of the sought-after unknowns is facilitated through the resolution of a system of equations. The empirical determination of the range of relaxation times is a prevalent practice, typically expanded by one or two orders of magnitude. Previous scholarly investigations frequently relied upon the formulation presented in Equations (8) and (9) to express the relaxation time, contributing to the established body of knowledge in the field:

$$\rho_{\min} = e^{A\pi/2}/\omega_{\max}, \rho_{\max} = e^{-A\pi/2}/\omega_{\min} \tag{8}$$

$$\rho_n = k \times 10^{(n-c)} \tag{9}$$

where $\omega_{\min}$ and $\omega_{\max}$ represent the frequency range of the determined storage modulus, we take $A = 0$ in this study to expand the order of magnitude. Generally, k is taken as 2.

Through the computation of the Prony series parameters and subsequent substitution into Equation (6), the relaxation modulus is derived at various relaxation time stages, forming the principal relaxation modulus curve. The comparative analysis, illustrated in Figure 8 and drawing insights from prior studies [22,25] addressing the relaxation modulus in both conventional asphalt mixtures and SMA-13, highlights notable distinctions. Specifically, the rate of decay from the upper limit stable value to the lower limit stable value under investigation, referred to as PSFM, is observed to be 16.8% slower than that of SMA-13 and 8% faster than the conventional asphalt mixture. It can be seen from previous studies that the faster the attenuation rate of the relaxation modulus of the material, the stronger the low-temperature crack resistance. Consequently, the findings suggest that PSFM exhibits heightened resistance to cracking at low temperatures compared with the conventional asphalt mixture, albeit not as robust as SMA-13 in this regard.

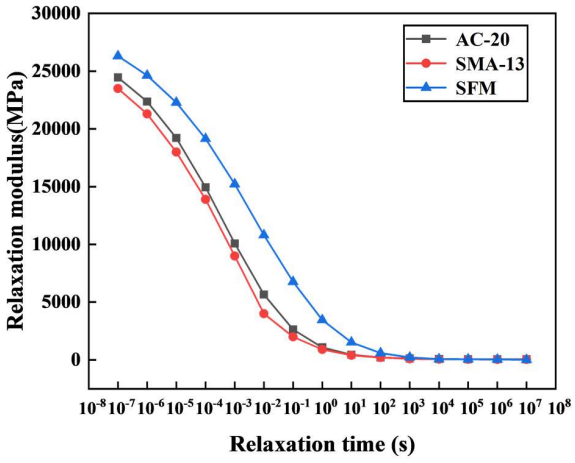

Figure 8. Relaxation modulus master curve.

3.3. Temperature Shrinkage Coefficient

To determine the temperature shrinkage coefficient of cement-based grouting material, it is necessary to calculate the weighted average of these coefficients according to the temperature range coefficients obtained in Table 6. Each coefficient related to a specific temperature range is multiplied by the corresponding temperature span, and then the obtained values are accumulated and summed. Subsequently, this cumulative sum is divided by the total span encompassing all temperature ranges. Through this method, the weighted average thermal contraction coefficient is obtained. In the case of cement-based grouting material, the resultant temperature shrinkage coefficient is determined to be $10.5 \times 10^{-6}/°C$. This rigorous methodology ensures a comprehensive and accurate representation of the material's response to temperature variations.

Table 6. Temperature contraction coefficients at various temperature intervals.

Temperature Range (°C)	−25~−15 °C	−15~−10 °C	−10~−5 °C	−5~0 °C	0~5 °C	5~10 °C	10~15 °C
Temperature contraction coefficient ($\times 10^{-6}/°C$)	10.8	10.1	9.5	11.0	9.3	12.0	10.7

4. Low-Temperature Stress Analysis of SFP

For the low-temperature stress analysis of SFP, different combinations of pavement structures are designed by first considering different application layers and thicknesses of the PSFM, and the pavement structure model is created by using the COMSOL Multiphysics 5.6 finite element analysis software to simulate the temperature field distribution of the whole pavement structure under different temperature conditions, respectively. The low-temperature stresses generated in the pavement structure by the simulated temperature distribution are analyzed using appropriate stress analysis techniques.

4.1. Finite Element Modelling

Before the low-temperature stress analysis of SFP, the finite element modeling of pavement structure is carried out to determine the geometric shape of pavement structure and the material properties of each layer. The accuracy of the analysis is increased by meshing. In order to meet the requirements of the actual pavement structure, the boundary conditions are specified for the model.

4.1.1. Structural Form

The primary objective of this investigation is to enhance the resistance of asphalt pavements to low-temperature cracking in cold regions by strategically designing pavement structures that incorporate PSFM. Departing from a conventional double-layer asphalt pavement structure as the baseline, PSFM is judiciously integrated into both the wearing layer and the binder layer. To explore the influence of varying layer thicknesses, 11 distinct pavement structure configurations were formulated, as detailed in Table 6. These configurations were systematically subjected to simulation and analysis. Notably, structures denoted as A to E incorporate PSFM in the wearing layer, while those labeled as a to e feature PSFM in the binder layer. This comprehensive approach aims to assess the effectiveness of PSFM in mitigating low-temperature cracking across diverse pavement configurations, contributing valuable insights for SFP performance in cold climates.

4.1.2. Geometric Modeling

In the analysis of temperature-induced stresses, the theoretical framework for numerical simulation rests upon the principles governing a viscoelastic layered system in the context of road structures. A comprehensive three-dimensional finite element model is devised, guided by specific assumptions [41]. In this model, the pavement-wearing layer is assumed to exhibit uniform isotropic viscoelastic behavior, while the remaining layers are treated as linearly elastic. Assumptions also encompass seamless bonding and con-

tinuous displacement between individual structural layers, ensuring consistent interlayer temperature and heat flux. The analytical approach disregards lateral variations in the pavement temperature field and simplifies heat flow as unidirectional, perpendicular to the pavement direction. Notably, it neglects the impact of temperature alterations on the thermal conductivity of each layer of material.

Acknowledging the strip-like configuration of the pavement structure, characterized by infinite longitudinal (driving direction) and depth dimensions but relatively confined transverse dimensions, the challenge arises in defining finite dimensions for the computational model. Due to practical limitations, infinite dimensions cannot be practically employed in the modeling process. Hence, the computational model's dimensions are meticulously determined to strike a balance between computational accuracy and complexity. Adhering to the precision requirements of the study, the model's pavement plane direction is set at a 4 m × 4 m square, incorporating layer thicknesses as per Table 7 and a soil depth of 5 m. This delineates the establishment of a three-dimensional geometric representation of the pavement structure, as illustrated in Figure 9.

Table 7. Different pavement structure combinations.

Typology	Pavement Structure Combination
Typical structure	5 cm SMA-13 + 7 cm AC-20 + 40 cm cement stabilized macadam + 15 cm natural gravel
Comparative structures, *A*	5 cm PSFM + 7 cm AC-20 + 40 cm cement stabilized macadam + 15 cm natural gravel
Comparative structures, *B*	4 cm PSFM + 7 cm AC-20 + 40 cm cement stabilized macadam + 15 cm natural gravel
Comparative structures, *C*	6 cm PSFM + 7 cm AC-20 + 40 cm cement stabilized macadam + 15 cm natural gravel
Comparative structures, *D*	5 cm PSFM + 6 cm AC-20 + 40 cm cement stabilized macadam + 15 cm natural gravel
Comparative structures, *E*	5 cm PSFM + 8 cm AC-20 + 40 cm cement stabilized macadam + 15 cm natural gravel
Comparative structures, *a*	5 cm SMA-13 + 7 cm PSFM + 40 cm cement stabilized macadam + 15 cm natural gravel
Comparative structures, *b*	4 cm SMA-13 + 7 cm PSFM + 40 cm cement stabilized macadam + 15 cm natural gravel
Comparative structures, *c*	6 cm SMA-13 + 7 cm PSFM + 40 cm cement stabilized macadam + 15 cm natural gravel
Comparative structures, *d*	5 cm SMA-13 + 6 cm PSFM + 40 cm cement stabilized macadam + 15 cm natural gravel
Comparative structures, *e*	5 cm SMA-13 + 8 cm PSFM + 40 cm cement stabilized macadam + 15 cm natural gravel

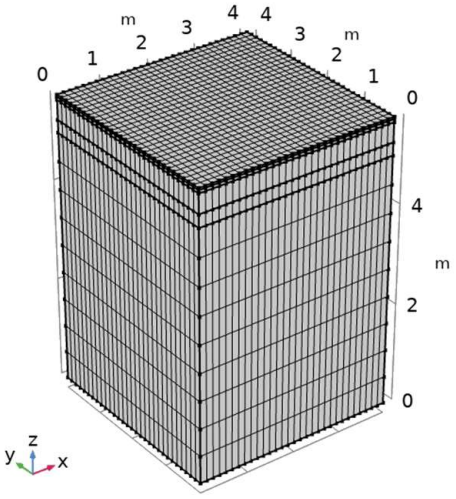

Figure 9. Three-dimensional pavement structure geometry model.

4.1.3. Material Parameters

Based on the above test results and the pavement material parameter data from the cited studies [42,43], the material parameters collated in Table 8 were imported into the geometric model in Figure 8 (Section 3.2) for subsequent low-temperature stress analysis.

Table 8. Pavement material parameters.

Materials	Poisson's Ratio	Thermal Conductivity (kcal/(m·h·°C))	Densities (kg/m^3)	Specific Heat Capacity (J/kg·K)
SMA-13	0.35	1.5	2560	1000
PSFM	0.3	1.2	2600	900
AC-20	0.25	1.1	2300	925
Cement-stabilized macadam	0.2	1.3	2200	911
Natural gravel	0.2	1.1	1374	942

4.1.4. Boundary Condition

Symmetric boundary conditions have been meticulously imposed on the geometric model depicted in Figure 8, representing the pavement structure. Defined displacements are judiciously specified in both the transverse and longitudinal directions to ensure a comprehensive characterization of the system's response. The lower boundary is subjected to fixed conditions, thereby constraining its movement, while the upper boundary of the pavement structure is intricately configured to facilitate surface-to-surface radiation heat transfer mechanisms.

To establish a well-defined thermal environment, the initial temperature at the bottom boundary is rigorously set to 0 °C, emphasizing a controlled starting point. Concurrently, the remaining boundaries are systematically demarcated as thermally insulated, ensuring an encapsulated and controlled thermal regime within the computational domain.

In regions where the load interacts with the pavement, a judiciously chosen dense mesh is employed, enhancing computational resolution and precision to accurately capture localized effects. Conversely, in areas devoid of direct contact, a strategically sparse mesh is implemented, optimizing computational efficiency without compromising the fidelity of the numerical simulation. This meshing strategy aims to strike a balance between computational resource utilization and the accurate representation of physical phenomena within the pavement structure.

4.2. Low-Temperature Stress Calculation Method

This study employs the COMSOL finite element software to ascertain temperature-induced stresses in asphalt pavement structures. The investigation adheres to the foundational principles of heat conduction theory, incorporating considerations of the thermal properties intrinsic to the structure. Furthermore, the initial and boundary conditions are meticulously considered during the computational process, where temperatures at diverse points within the structure are computed for each temporal instance. This computational procedure serves to establish the internal temperature field of the pavement.

In the subsequent analysis of the temperature field, it is acknowledged that setting initial temperatures uniformly to 0 °C, while a common practice, may not precisely capture the authentic temperature distribution. Upon the stabilization of the internal temperature field following a designated period of temperature influence, it is employed as the foundational input for the subsequent low-temperature stress analysis.

In the transient finite element analysis considering the stress relaxation of the pavement material and the variable temperature field, this study comprehensively considers and finds that the temperature field changes slowly. It first considers the stress relaxation effect of the material by setting the step size [0, 0.01, 1] and transient analysis of the pavement structure. After considering the temperature field variation, a larger step size is later set, and a 24 h temperature field analysis is carried out by setting every hour as a unit.

Variations in regional climates engender considerable diversity in pavement temperature fields, consequently affecting the internal low-temperature stress experienced by asphalt pavements. Recent investigations have focused on examining the temperature distribution within asphalt pavements in cold regions. These studies specifically scrutinize the average low temperatures during winter in such regions, alongside exploring extreme

low-temperature conditions. The environmental attributes pertinent to these investigations are delineated in Table 9.

Table 9. Climatic conditions.

	Average Low Temperature T_1 (°C)	Extreme Low Temperatures T_2 (°C)	Average Daily Maximum Solar Radiation at Noon (W/m^2)
Climatic conditions	−6~−18	−13~−28	626

4.3. Low-Temperature Stresses in SFP

4.3.1. Effect of Different Applied Layers on Low-Temperature Stresses

In the context of varying temperature conditions, an examination of low-temperature stresses across different layers of the pavement structure is conducted under conditions representing the most unfavorable scenarios. As depicted in Figure 10, it is evident that the wearing layer is particularly susceptible to experiencing heightened low low-temperature stress. Progressing in the depth direction, the influence of temperature fluctuations and material properties on low-temperature stresses diminishes, exhibiting minimal impact on the base and subbase layers.

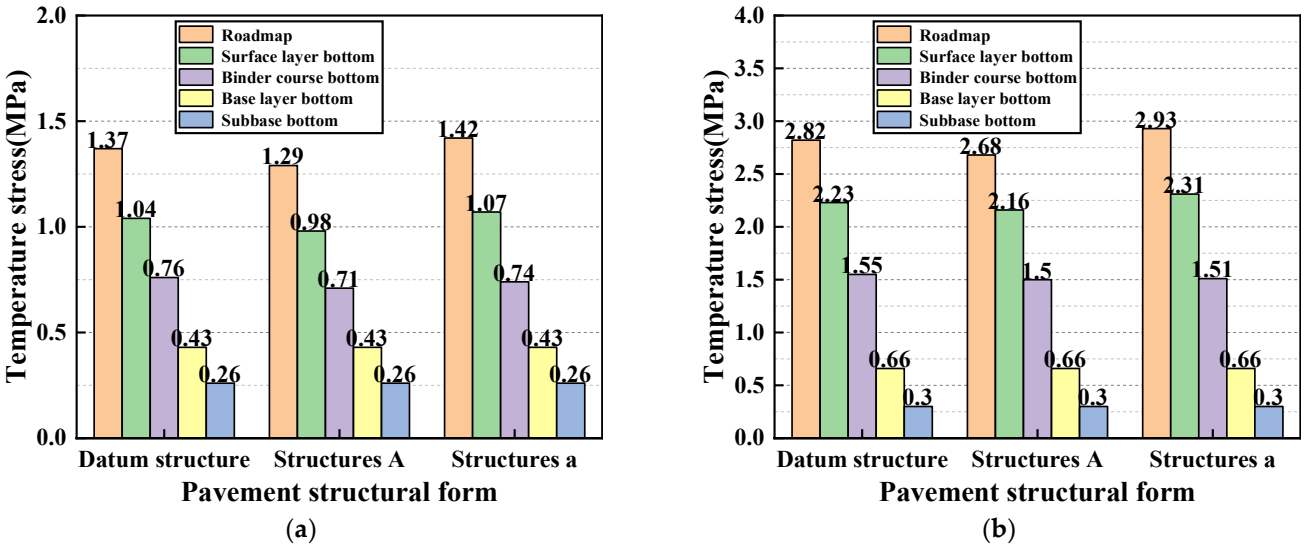

Figure 10. Low-temperature stress distribution in different structures under different temperature conditions; (**a**) comparison of low-temperature stresses at T_1; and (**b**) comparison of low-temperature stresses at T_2.

Comparatively, when juxtaposed with the typical pavement structure, the low low-temperature stress on the road surface under T_1 is mitigated by 0.08 MPa in Comparative Structures A. Furthermore, the low low-temperature stress at the bottom of the wearing layer shows a reduction of 0.06 MPa, while the low low-temperature stress at the bottom of the binder layer decreases by 0.05 MPa. Similarly, under T_2 conditions, Comparative Structures A manifest a reduction of 0.14 MPa in road surface low low-temperature stress, a decrease of 0.07 MPa at the bottom of the wearing layer, and a 0.05 MPa decline in low-temperature stress at the bottom of the binder layer.

In contrast, Comparative Structures a, when compared with the reference typical pavement structure, exhibit nuanced variations in low-temperature stresses. Specifically, under T_1 conditions, the low-temperature stress at the road surface increases by 0.05 MPa, while at the bottom of the wearing layer, there is an increment of 0.03 MPa. Conversely, the low-temperature stress at the bottom of the binder layer decreases by 0.02 MPa. Similarly, under T_2 conditions, the low-temperature stress at the road surface rises by 0.11 MPa, the

bottom of the wearing layer experiences an increase of 0.08 MPa, and the bottom of the binder layer sees a reduction of 0.04 MPa.

Furthermore, an assessment of low low-temperature stress at the same temperature reveals notable distinctions when PSFM is employed as the wearing layer material. Specifically, the low low-temperature stress is 4.73% less than that of SMA-13 in the typical pavement structure, and concurrently, the low low-temperature stress on the internal binder layer material is reduced by 4.91%. Conversely, when utilized as the binder layer material, the low low-temperature stress is 2.61% less than that of AC-20 in the typical pavement structure. However, it results in a 3.5% increase in the low low-temperature stress on the wearing layer of SMA-13.

In summary, the analysis results indicate that employing PSFM as the wearing layer material minimizes low low-temperature stress experienced by the pavement structure at the same temperature. Conversely, when utilized as the binder layer material, while it reduces low-temperature stress within the binder layer, it concurrently elevates low-temperature stresses in the wearing layer material, rendering it more susceptible to low-temperature cracking.

4.3.2. Effect of Different Surface Thicknesses on Low-Temperature Stresses

In this section, the pavement structure configuration outlined in Table 7 is employed, utilizing PSFM as both the wearing layer and binder layer material. The analysis focuses on varying the thicknesses of the wearing layer to assess the low-temperature stress distribution within the pavement structure under T_2 conditions. It is notable that altering the wearing layer material has minimal impact on the low-temperature stresses at the bottom of the roadbed and the sub-base layer. Therefore, the investigation in this section concentrates solely on the low-temperature stress distribution within the wearing layer.

The findings indicate that, when the thickness of the PSFM wearing layer is increased from 4 cm to 6 cm within the asphalt pavement configuration, depicted in Figure 11, several changes in low-temperature stresses are observed. Specifically, as the wearing layer thickness escalates, the surface low-temperature stress rises by 0.05 MPa, while the low-temperature stress at the bottom of the wearing layer decreases by 0.04 MPa. Simultaneously, the low-temperature stress at the bottom of the binder layer decreases by 0.02 MPa in correlation with the increase in the wearing layer thickness. Additionally, maintaining a constant wearing layer thickness while increasing the binder layer thickness from 6 cm to 8 cm yields specific variations in low-temperature stresses. Consequently, the low-temperature stress at the bottom of the binder layer decreases by 0.02 MPa in tandem with the increase in wearing layer thickness. Similarly, keeping the wearing layer thickness constant and augmenting the binder layer thickness from 6 cm to 8 cm manifests distinct alterations in low-temperature stresses. This scenario results in an increase of 0.04 MPa in road surface low-temperature stress. Meanwhile, the low-temperature stress at the bottom of the wearing layer decreases by 0.02 MPa, and the low-temperature stress at the bottom of the binder layer decreases by 0.01 MPa.

In the utilization of PSFM as the binder layer, as illustrated in Figure 12, an examination of thickness variations from 6 cm to 8 cm reveals noteworthy changes in low-temperature stresses across different layers. Specifically, there is an observed increase of 0.06 MPa in the low-temperature stress at the road surface, concomitant with a decrease of 0.03 MPa in the low-temperature stress at the bottom of the wearing layer, and a decrease of 0.02 MPa in the low-temperature stress at the bottom of the binder layer. Conversely, maintaining the thickness of the binder layer constant while increasing the thickness of the wearing layer from 4 cm to 6 cm results in an elevation of 0.06 MPa in road surface low-temperature stress. Simultaneously, a decrease of 0.05 MPa in the low-temperature stress at the bottom of the wearing layer and a decrease of 0.01 MPa at the bottom of the binder layer is noted.

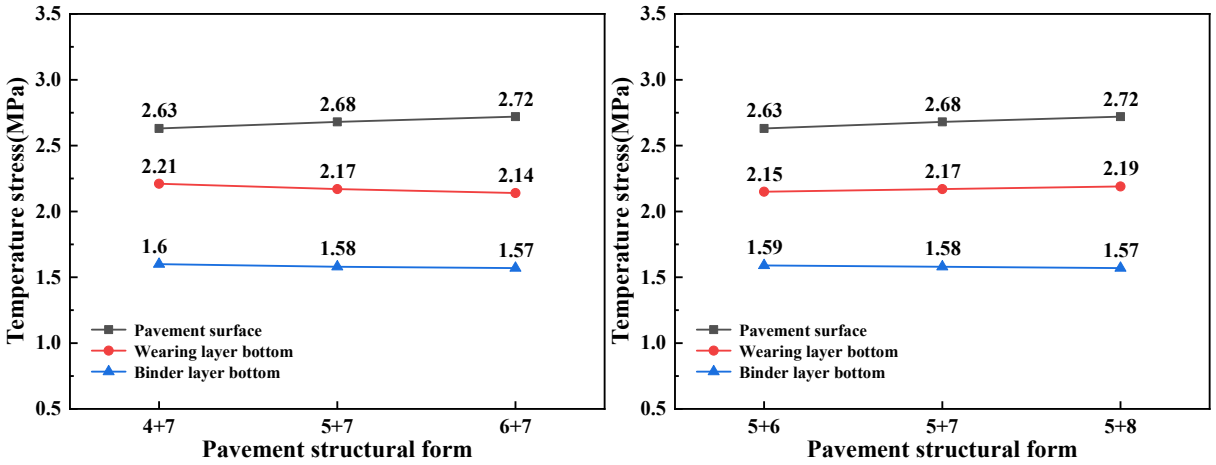

Figure 11. Low-temperature stress distribution of different pavement structural forms with PSFM as the wearing layer material.

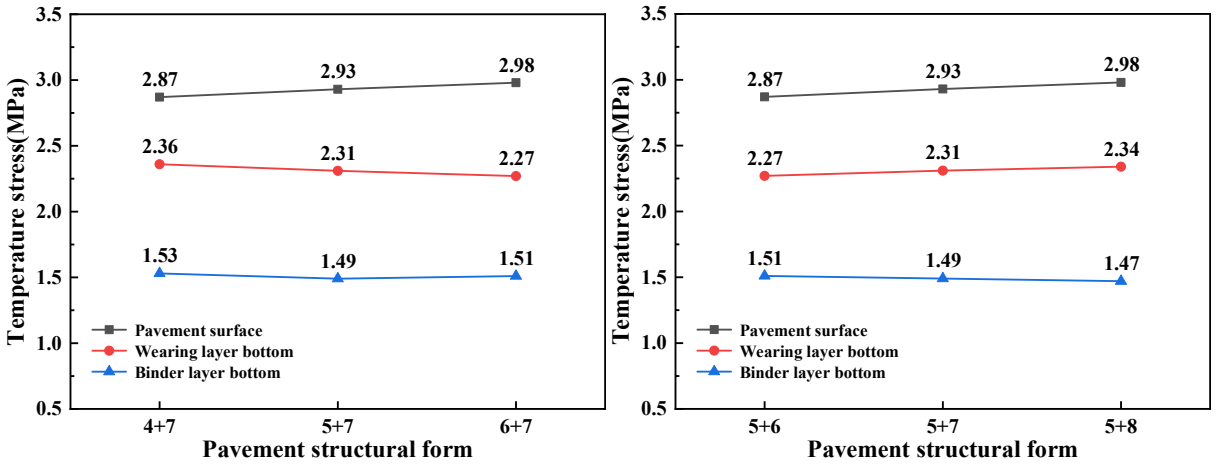

Figure 12. Low-temperature stress distribution of different pavement structural forms with PSFM as the binder layer material.

The analysis yields the conclusion that augmenting the thickness of the pavement-wearing layer correlates with an escalation in thermal stress on the pavement surface. However, the influence of varying the thickness of different layers on internal low-temperature stress is nuanced. Specifically, when PSFM serves as the binder layer, an increase in binder layer thickness introduces differences in modulus, leading to an augmentation of low-temperature stress in the wearing layer (SMA-13). Conversely, maintaining the thickness of the binder layer while increasing the thickness of the wearing layer proves effective in mitigating internal low-temperature stress, albeit at the expense of an increase in low-temperature stress at the road surface.

5. Discussion

As a pavement material, PSFM has many advantages, which makes it widely used. First, the initial cost of PSFM is higher, but the long-term maintenance cost is lower, which can save maintenance and repair costs. The initial cost of asphalt mixture is lower, but the long-term maintenance cost is higher, which requires more frequent repair and maintenance. In addition, PSFM also has a longer service life and better durability, which can be used in a wider temperature range and can better adapt to climate change and traffic load changes. In the field of road engineering, PSFM has often been utilized to alleviate rutting in asphalt pavements subjected to high temperatures, either as a wearing layer material or

below. However, when used as the binder layer material in cold climates, an elevation in temperature-induced cracks has been detected.

To rectify this problem and enhance the crack resistance of SFP at low temperatures, a series of comprehensive studies (referenced as [44–47]) have been conducted. These investigations focus on enhancing the innate crack resistance of PSFM through various interventions. The addition of additives to cement-based grouting material involves tailored modifications to improve crack resistance. Similarly, the introduction of emulsified asphalt seeks to enhance low-temperature crack resistance by modifying the binder composition for improved flexibility in cold conditions. Efforts are also directed toward optimizing the structure of porous asphalt mixtures, with meticulous adjustments made to the arrangement of aggregates and void spaces within the mixture to improve crack resistance.

However, it is important to recognize that these efforts, although effective in improving low-temperature crack resistance, often involve a trade-off. The optimization measures used to mitigate cold-induced cracking can inadvertently reduce resistance to high-temperature deformations. This highlights the complexity of addressing different performance criteria in asphalt pavement design, requiring a careful and comprehensive approach to tackle the multifaceted challenges presented by varying environmental conditions.

In studies examining crack resistance in asphalt pavements, finite element software is commonly employed to simulate the distribution of internal low-temperature stress within the pavement structure. This approach aims to forecast asphalt mixture shrinkage at low temperatures [48–51]. However, there is a notable gap in low-temperature stress analysis specifically focused on the use of PSFM. This lack of understanding presents challenges in proposing precise design parameters during the pavement structure design phase, as the incorporation of multiple materials introduces complexity. Consequently, pavement structures are frequently inadequately verified, impeding the optimization of pavement designs.

Although PSFM is effective in mitigating various issues as a binder layer material, its usage in cold regions has been found to result in a significant increase in transverse cracks on the wearing layer due to low low-temperature stress. To address low-temperature cracking, some pavement structures use PSFM as the binder layer material while increasing the thickness of the wearing layer to reduce low-temperature stress within the pavement structure. However, this results in elevated low-temperature stress on the pavement surface. These complexities can be addressed through material development strategies aimed at enhancing the crack resistance of the SMA-13 wearing layer.

This analysis focuses on the stress relaxation of asphalt mixtures and the thermal shrinkage strain of cement-based grouting material, but further refinement is necessary to enhance material property analysis rigor. This involves a meticulous examination of bonding effects between cement-based grouting material and asphalt at microscopic levels across different temperatures, considering factors such as grout shrinkage. Assessing the sensitivity of various material parameters to temperature-induced stresses is also crucial. To achieve these objectives, this study conducts a comprehensive low-temperature stress analysis based on indoor experimental data. By incorporating precise material parameters, the goal is to establish a robust foundation for the widespread application of SFPs in cold regions.

6. Conclusions

This investigation uses PSFM as either the wearing layer material or binder layer material, exploring low-temperature stress distribution through different combinations of layer thicknesses and structural configurations. COMSOL finite element simulation is employed to analyze these behaviors and thermal interactions, known for its efficacy in capturing intricate structural behaviors.

(1) When PSFM is used as the wearing layer material, it experiences 4.7% lower low-temperature stresses compared with a conventional pavement structure under the same thermal conditions. It also effectively reduces low-temperature stress on the binder layer

material by 6.4%. Conversely, when used as the binder layer material, PSFM reduces low-temperature stress by 3% compared with the binder layer of a typical pavement structure (AC-20). However, it is important to note that the low-temperature stress on the SMA-13 wearing layer increases by 3.5%, making it more susceptible to low-temperature cracking in this specific layer.

(2) Increasing the thickness of the pavement wearing layer intensifies surface low-temperature stress, but the effect on internal low-temperature stress varies across different layers. When PSFM is used as the wearing layer material, its resistance to low-temperature stress increases with thicker layers, leading to a rise in surface low-temperature stress and an increased risk of temperature-induced cracks. However, internal low-temperature stress decreases by 1.3%. Conversely, when PSFM is used as the binder layer material, increasing the binder layer thickness results in higher low-temperature stress in the SMA-13 wearing layer due to differences in modulus. Maintaining the binder layer thickness while increasing the wearing layer thickness reduces internal low-temperature stress by 1.3% while raising pavement surface low-temperature stress by 1.9%.

To address low-temperature cracking in colder climates, the low-temperature stress analysis suggests using PSFM as the binder layer material and increasing the thickness of the wear layer. This adjustment significantly reduces low-temperature stresses in the wearing layer, effectively mitigating the risk of low-temperature cracking.

Author Contributions: Conceptualization, G.L. and H.Z.; methodology, G.L. and H.Z.; software, D.W., H.Z., B.X., F.Y. and Z.Z.; validation, G.L., D.W., H.Z. and Z.Z.; formal analysis, G.L., D.W. and H.Z.; investigation, D.W., H.Z., B.X., F.Y. and Z.Z.; data curation, B.X., F.Y. and Z.Z.; writing—original draft preparation, G.L. and D.W.; writing—review and editing, H.Z., F.Y. and Z.Z.; supervision, H.Z. All authors have read and agreed to the published version of the manuscript.

Funding: This study is supported by the technology development projects from the China First Highway Engineering Co., Ltd., grant number T-SZ-S4GS(J)-SIC-WRL-00-QT-011.

Data Availability Statement: Data are contained within the article.

Acknowledgments: This research was conducted at Shenyang Jianzhu University.

Conflicts of Interest: Author Guoxun Li, Deyong Wang, Biao Xu were employed by the company China First Highway Engineering Co., Ltd. Author Fan Yang was employed by the company CCCC Comprehensive Planning and Design Institute Co., Ltd. The remaining authors declare that the research was conducted in the absence of any commercial or financial relationships that could be construed as a potential conflict of interest. The authors declare that this study received funding from China First Highway Engineering Co., Ltd. The funder was not involved in the study design, collection, analysis, interpretation of data, the writing of this article or the decision to submit it for publication.

References

1. Ling, S.; Hu, M.; Sun, D.; Ni, H.; Xu, L. Mechanical properties of pouring semi-flexible pavement material and engineering estimation on contribution of each phase. *Constr. Build. Mater.* **2022**, *315*, 125782. [CrossRef]
2. Zarei, S.; Alae, M.; Ouyang, J.; Zhao, Y. Rutting and surface-initiated cracking mechanisms of semi-flexible pavements with cement asphalt emulsion pastes. *Int. J. Pavement Eng.* **2022**, *24*, 1–15. [CrossRef]
3. Yang, B.; Weng, X. The influence on the durability of semi-flexible airport pavement materials to cyclic wheel load test. *Constr. Build. Mater.* **2015**, *98*, 171–175. [CrossRef]
4. Luo, S.; Yang, X.; Zhong, K.; Yin, J. Open-graded asphalt concrete grouted by latex modified cement mortar. *Road Mater. Pavement Des.* **2020**, *21*, 61–77. [CrossRef]
5. Hassani, A.; Taghipoor, M.; Karimi, M.M. A state of the art of semi-flexible pavements: Introduction, design, and performance. *Constr. Build. Mater.* **2020**, *253*, 119196. [CrossRef]
6. Khan, M.I.; Huat, H.Y.; Dun, M.H.b.M.; Sutanto, M.H.; Jarghouyeh, E.N.; Zoorob, S.E. Effect of irradiated and non-irradiated waste PET based cementitious grouts on flexural strength of semi-flexible pavement. *Materials* **2019**, *12*, 4133. [CrossRef]
7. Moghaddam, T.B.; Karim, M.R.; Abdelaziz, M. A review on fatigue and rutting performance of asphalt mixes. *Sci. Res. Essays* **2011**, *6*, 670–682.
8. Xu, T.; Huang, X. Investigation into causes of in-place rutting in asphalt pavement. *Constr. Build. Mater.* **2012**, *28*, 525–530. [CrossRef]

9. Cai, J.; Pei, J.; Luo, Q.; Zhang, J.; Li, R.; Chen, X. Comprehensive service properties evaluation of composite grouting materials with high-performance cement paste for semi-flexible pavement. *Constr. Build. Mater.* **2017**, *153*, 544–556. [CrossRef]
10. Asim, M.; Ahmad, M.; Alam, M.; Ullah, S.; Iqbal, M.J.; Ali, S. Prediction of rutting in flexible pavements using finite element method. *Civ. Eng. J.* **2021**, *7*, 1310–1326. [CrossRef]
11. Ding, Q.; Zhao, M.; Shen, F.; Zhang, X. Mechanical behavior and failure mechanism of recycled semi-flexible pavement material. *J. Wuhan Univ. Technol.-Mater. Sci. Ed.* **2015**, *30*, 981–988. [CrossRef]
12. Wang, S.; Zhou, H.; Chen, X.; Gong, M.; Hong, J.; Shi, X. Fatigue resistance and cracking mechanism of semi-flexible pavement mixture. *Materials* **2021**, *14*, 5277. [CrossRef]
13. Khan, M.I.; Sutanto, M.H.; Yusoff, N.I.M.; Zoorob, S.E.; Rafiq, W.; Ali, M.; Fediuk, R.; Vatin, N.I. Cementitious grouts for semi-flexible pavement surfaces—A review. *Materials* **2022**, *15*, 5466. [CrossRef]
14. Hou, S.; Xu, T.; Huang, K. Investigation into engineering properties and strength mechanism of grouted macadam composite materials. *Int. J. Pavement Eng.* **2016**, *17*, 878–886. [CrossRef]
15. Wang, D.; Liang, X.; Li, D.; Liang, H.; Yu, H. Study on mechanics-based cracking resistance of semiflexible pavement materials. *Adv. Mater. Sci. Eng.* **2018**, *2018*, 8252347. [CrossRef]
16. Jiang, D.; Wang, D.; Chen, Z.; Fan, L.; Yi, J. Research on the mesoscopic viscoelastic property of semi-flexible pavement mixture based on discrete element simulation. *Case Stud. Constr. Mater.* **2022**, *17*, e01282. [CrossRef]
17. Xiong, Z.; Gong, M.; Hong, J.; Zhang, L. An investigation on failure behavior of semi-flexible composite mixture at different temperatures. *J. Road Eng.* **2023**, *3*, 186–202. [CrossRef]
18. Luo, Y.; Wu, H.; Song, W.; Yin, J.; Zhan, Y.; Yu, J.; Wada, S.A. Thermal fatigue and cracking behaviors of asphalt mixtures under different temperature variations. *Constr. Build. Mater.* **2023**, *369*, 130623. [CrossRef]
19. Mead, D. Determination of molecular weight distributions of linear flexible polymers from linear viscoelastic material functions. *J. Rheol.* **1994**, *38*, 1797–1827. [CrossRef]
20. Fang, N.; Li, H.; Li, Q.; Wang, X.; Hu, S.; Xin, L. Study on asphalt layer of composite pavement temperature shrinkage stress considering stress relaxation. *Mater. Struct.* **2021**, *54*, 32. [CrossRef]
21. Kuchiishi, A.K.; Santos Antão, C.C.d.; Vasconcelos, K.; Bernucci, L.L.B. Influence of viscoelastic properties of cold recycled asphalt mixtures on pavement response by means of temperature instrumentation. *Road Mater. Pavement Des.* **2019**, *20*, S710–S724. [CrossRef]
22. Stimilli, A.; Virgili, A.; Canestrari, F.; Bahia, H.U. Estimation of low-temperature performance of recycled asphalt mixtures through relaxation modulus analysis. *Cold Reg. Sci. Technol.* **2017**, *133*, 36–45. [CrossRef]
23. Song, S.H. Fracture of Asphalt Concrete: A Cohesive Zone Modeling Approach Considering Viscoelastic Effects. Ph.D. Thesis, University of Illinois at Urbana-Champaign, Champaign, IL, USA, 2006.
24. Yu, D.; Yu, X.; Gu, Y. Establishment of linkages between empirical and mechanical models for asphalt mixtures through relaxation spectra determination. *Constr. Build. Mater.* **2020**, *242*, 118095. [CrossRef]
25. Liu, H.; Luo, R.; Lv, H. Establishing continuous relaxation spectrum based on complex modulus tests to construct relaxation modulus master curves in compliance with linear viscoelastic theory. *Constr. Build. Mater.* **2018**, *165*, 372–384. [CrossRef]
26. Jian-long, Z.; Guo-ping, Q.; Rong-hua, Y. Testing thermalviscoelastic constitutive relation of asphalt mixtures and its mechanical applications. *Eng. Mech.* **2008**, *25*, 34-041.
27. Liu, H.; Zeiada, W.; Al-Khateeb, G.G.; Shanableh, A.; Samarai, M. A framework for linear viscoelastic characterization of asphalt mixtures. *Mater. Struct.* **2020**, *53*, 32. [CrossRef]
28. Li, G.; Xiong, H.; Ren, Q.; Zheng, X.; Wu, L. Experimental Study and Performance Characterization of Semi-Flexible Pavements. *Coatings* **2022**, *12*, 241. [CrossRef]
29. Zhang, W.; Cui, B.; Gu, X.; Dong, Q. Comparison of relaxation modulus converted from frequency-and time-dependent viscoelastic functions through numerical methods. *Appl. Sci.* **2018**, *8*, 2447. [CrossRef]
30. Zhao, Y.; Ni, Y.; Zeng, W. A consistent approach for characterising asphalt concrete based on generalised Maxwell or Kelvin model. *Road Mater. Pavement Des.* **2014**, *15*, 674–690. [CrossRef]
31. Mateos, A.; Harvey, J.; Feldman, D.R.; Wu, R.; Paniagua, J.; Paniagua, F. Evaluation of the moisture dependence of concrete coefficient of thermal expansion and its impacts on thermal deformations and stresses of concrete pavements. *Transp. Res. Rec.* **2020**, *2674*, 545–555. [CrossRef]
32. Hao, P.; Zhang, L. Asphalt pavement low-temperature stress analysis based on continuous variable temperatures. *J. Xi'an Univ. Archit. Technol.* **2018**, *50*, 176–183.
33. Hills, J.; Brien, D. The fracture of bitumens and asphalt mixes by temperature induced stresses. In Proceedings of the Association of Asphalt Paving Technologists, Minneapolis, MN, USA, 1966; pp. 292–309.
34. Geng, L.; Wang, X.; Xu, Q. Thermal stress of asphalt pavement based on dynamic characteristics of asphalt mixtures. *Int. J. Pavement Res. Technol.* **2016**, *9*, 363–367. [CrossRef]
35. Si, C.; Chen, E.; You, Z.; Zhang, R.; Qiao, P.; Feng, Y. Dynamic response of temperature-seepage-stress coupling in asphalt pavement. *Constr. Build. Mater.* **2019**, *211*, 824–836. [CrossRef]
36. Zhang, F.; Wang, L.; Li, C.; Xing, Y. Predict the phase angle master curve and study the viscoelastic properties of warm mix crumb rubber-modified asphalt mixture. *Materials* **2020**, *13*, 5051. [CrossRef] [PubMed]

37. Shan, L.; Tan, Y.; Zhang, H.; Xu, Y. Analysis of linear viscoelastic response function model for asphalt binders. *J. Mater. Civ. Eng.* **2016**, *28*, 04016010. [CrossRef]
38. Findley, W.N.; Davis, F.A. *Creep and Relaxation of Nonlinear Viscoelastic Materials*; Courier Corporation: Chelmsford, MA, USA, 2013.
39. Schapery, R.A. Correspondence principles and a generalized J integral for large deformation and fracture analysis of viscoelastic media. *Int. J. Fract.* **1984**, *25*, 195–223. [CrossRef]
40. Xi, L.; Luo, R.; Ma, Q.; Tu, C.; Shah, Y.I. An improved method to establish continuous relaxation spectrum of asphalt materials. *Constr. Build. Mater.* **2022**, *354*, 129182. [CrossRef]
41. Yu, X.; Luo, R.; Huang, T.; Wang, J.; Chen, Y. Dielectric properties of asphalt pavement materials based on the temperature field. *Constr. Build. Mater.* **2021**, *303*, 124409. [CrossRef]
42. Chen, J.; Li, Z.; Zhao, Z.; Huang, X.; Chen, J.; Liu, Z. Investigation on temperature shrinkage characteristics of the combined structure in asphalt pavement. *Front. Mater.* **2022**, *9*, 1055641.
43. Wang, Y.; Zhang, L. Low doses of cement stabilized macadam roadbase-shrinkage performance research. *J. Liaoning Tech. Univ.* **2016**, *35*, 283–288.
44. Yang, Q.; Zhao, W. Research on the crack resistance of semi-flexible pavement based on bonding and rheological properties of asphalt. *Constr. Build. Mater.* **2022**, *356*, 129093. [CrossRef]
45. Wang, D.; Liang, X.; Jiang, C.; Pan, Y. Impact analysis of Carboxyl Latex on the performance of semi-flexible pavement using warm-mix technology. *Constr. Build. Mater.* **2018**, *179*, 566–575. [CrossRef]
46. Fang, L.; Zhou, J.; Yang, Z.; Yuan, Q.; Que, Y. Interaction between cement and asphalt emulsion and its influences on asphalt emulsion demulsification, cement hydration and rheology. *Constr. Build. Mater.* **2022**, *329*, 127220. [CrossRef]
47. Davoodi, A.; Esfahani, M.A.; Bayat, M.; Mohammadyan-Yasouj, S.E. Evaluation of performance parameters of cement mortar in semi-flexible pavement using rubber powder and nano silica additives. *Constr. Build. Mater.* **2021**, *302*, 124166. [CrossRef]
48. Zarei, S.; Ouyang, J.; Zhao, Y. Evaluation of fatigue life of semi-flexible pavement with cement asphalt emulsion pastes. *Constr. Build. Mater.* **2022**, *349*, 128797. [CrossRef]
49. Somani, P.; Gaur, A. RETRACTED: Evaluation and reduction of low-temperature stresses in concrete pavement by using phase changing material. *Mater. Today* **2020**, *32*, 856–864.
50. Tang, J.; Fu, Y.; Ma, T.; Zheng, B.; Zhang, Y.; Huang, X. Investigation on low-temperature cracking characteristics of asphalt mixtures: A virtual thermal stress restrained specimen test approach. *Constr. Build. Mater.* **2022**, *347*, 128541. [CrossRef]
51. Sun, Y.; Zhang, Z.; Gong, H.; Zhou, C.; Chen, J.; Huang, B. 3D Multiscale modeling of asphalt pavement responses under coupled temperature–stress fields. *J. Eng. Mech.* **2022**, *148*, 04022010. [CrossRef]